IEEE Access
Multidisciplinary | Rapid Review | Open Access Journal

Received 30 December 2023, accepted 17 January 2024, date of publication 30 January 2024, date of current version 5 February 2024.

Digital Object Identifier 10.1109/ACCESS.2024.3359168

RESEARCH ARTICLE

Bandwidth, Gain Improvement, and Notched-Band Frequency of SWB Wave Coplanar Vivaldi Antenna Using CSRR

NURHAYATI NURHAYATI[1], (Member, IEEE), FITRI YULI ZULKIFLI[2], (Senior Member, IEEE), EKO SETIJADI[3], (Member, IEEE), BAGUS EDY SUKOCO[4], MOHD NAJIB MOHD YASIN[5], (Senior Member, IEEE), AND ALEXANDRE MANICOBA DE OLIVEIRA[6], (Member, IEEE)

[1]Department of Electrical Engineering, Universitas Negeri Surabaya, Surabaya 60231, Indonesia
[2]Department of Electrical Engineering, Universitas Indonesia, Depok 16435, Indonesia
[3]Department of Electrical Engineering, Institut Teknologi Sepuluh Nopember, Surabaya 60111, Indonesia
[4]National Research and Innovation Agency (BRIN), Electronics and Telecommunications Center, Bandung 40135, Indonesia
[5]Advanced Communication Engineering (ACE) Centre of Excellence, Faculty Electronic Engineering Technology, Universiti Malaysia Perlis (UniMAP), Kangar, Perlis 01000, Malaysia
[6]Laboratório James Clerk Maxwell de Micro-ondas e Eletromagnetismo Aplicado (LABMAX), Instituto Federal de Educacao, Ciencia e Tecnologia de Sao Paulo, Cubatão 11533-160, Brazil

Corresponding author: Nurhayati Nurhayati (nurhayati@unesa.ac.id)

This work was supported in part by the Indonesia Collaboration Research Funding from Legal-Entity State Higher Education Institutions (Universitas Negeri Surabaya, Universitas Indonesia, and Institut Teknologi Sepuluh Nopember); in part by Riset Kolaborasi Indonesia (RKI), Universitas Negeri Surabaya (Indonesia), under Grant B/38234/UN38.15/LK.04.00/2023; in part by the Collaboration Between the National Research and Innovation Agency, Bandung, Indonesia and Maxwell Laboratory, and Federal Institute of São Paulo (IFSP), Brazil; and we would like also acknowledge the support from the International Research Fund (INTERES) 9001-00032 UNIMAP-UNESA.

ABSTRACT Antennas with high gain that can operate in Super Wide Band (SWB) frequencies can be employed for a variety of wireless applications that serve different telecommunications infrastructure and radar applications. However, wide-bandwidth antennas suffer from interference from other wireless technology networks, necessitating the deployment of strategies to block some undesired signal frequencies. A new method for increasing bandwidth by shortening the taper slot length of the Vivaldi antenna and increasing the antenna radiation pattern by using a wavy structure and adding a Square-Complimentary Split Ring Resonator (S-CSRR) structure that can notched-band several frequencies has been investigated on the Coplanar Vivaldi Antenna (CVA). In this study, we investigated seven different types of antennas: Conventional CVA (C-CVA), CVA-Short Slot and Long-Slot (CVA-SS and CVA-LS) with antenna lengths of 10 and 15 cm, wave CVA (WCVA), and WCVA with CSRR. In all frequency bands ranging from 2.3 to more than 30 GHz, the S_{11} of the CVA-SS antenna is less than -15 dB with minimum S_{11} of -62.21 dB. When compared to the CVA-LS without a corrugated construction, the WCVA-SS antenna has 5.77 dBi improvement of directivity at 15 GHz. By incorporating the S-CSRR structure into WCVA, four notched frequency bands are formed: 3.335–3.72 GHz (WiMAX spectrum), 4.72 - 5.354 GHz (WLAN), 6.07–6.743 GHz (Wifi 6E usage), and 7.408–8.293 GHz (X- satellite bands). S-CSRR also potentially result in circular polarization at 4.6–5.3 GHz with the minimum AR of 0.438 (at 5 GHz), at 7.8 $-$8.2 GHz with the minimum AR of 0.732 (at 8GHz) and at 27 GHz with AR of 2.1 by constructing a U shape with four SCRRs. There was also good agreement between simulation and measurement results. As a result, the WCVA-SS antenna with a Square-CSRR structure may be recommended for the usage of SWB antennas, where a single antenna can serve numerous telecommunications and radar system applications.

The associate editor coordinating the review of this manuscript and approving it for publication was Tutku Karacolak.

INDEX TERMS Bandwidth, gain, notch-band, super wide band, Vivaldi antenna.

I. INTRODUCTION

Ultrawideband antennas have become popular for research and use in the wireless industry ever since the FCC allowed it to market communications in the 3.1-10.6 GHz frequency [1], [2], [3]. Ultrawideband antennas offer the benefit of enabling short-range wireless communications with high capacity while employing low-cost and low-energy transceivers. It should be noted that UWB short pulse signals can boost transmission speed, resist multipath fading and frequency selective fading, and provide excellent security and resolution for accurate indoor positioning systems [4], [5]. When compared to existing wireless technologies such as Bluetooth, UWB technology provides stronger localization capabilities and may be used for radar applications such as inside scanning and pin-pointing item positions and tracking [6], [7], [8]. UWB technology may be utilized for a variety of IoT [9], [10], automotive [11], and mobile applications [12]. Besides that, the need for communication using the Internet of Things (IoT) is also increasing, including wireless sensor networks, smart grids, control and automation systems, smart devices, and others [13], [14]. As communication demands evolve, so does the demand for mobile devices that can work in a variety of standards, be used in a variety of fading/interference settings, and be utilized for a variety of applications. To build this communication, the transceiver requires an antenna, preferably which has a small size and low fabrication.

Monopole and Vivaldi antennas are examples of antennas that can operate at frequencies with a broad bandwidth. Vivaldi antennas functioning at UWB frequencies have been studied in [15], [16], and [17], whereas Monopole antennas have been investigated in [18], [19], and [20]. Many Vivaldi antenna studies have been conducted to enhance bandwidth and gain such as Phased Adjusting Unit lens [21], Pseudoelement, corrugated [22], metasurface structure [23], dielectric load [24], and 4-dielectric layer [25]. However, some of these antennas are huge, difficult to build, and do not have a compact design due to the usage of lenses, many layers of substrate, and metasurface structures. Furthermore, some bandwidth impedance performance has not been satisfied since not all predicted frequencies in the required bandwidth goal have a VSWR of less than 2.

Nowadays, super-wideband (SWB) antennas are the main choice because they can cover various technological standards and reduce the overall size and weight of the device [26], [27]. UWB antennas have a Bandwidth Ratio (RBW) of 3.42:1 while antennas that have an RBW greater than 10:1 are classified as super wide band antennas (SWB) [13], [28]. A super-wideband antenna (SWB) can be the best choice as it includes several standards and wireless technologies in defense and security, which reduces the overall size/weight of the module whereby this SWB antenna can cover both short and long-range communications. The SWB antenna can support the use of a large number of wireless applications with a single device [29], [30]. SWB antenna technology can meet the demand for wireless sensors in various fields including the field of defense and security, and microwave imaging for surveillance [31] which can provide high data capacity, wide-coverage, higher Doppler resolution, high-resolution imaging, sensing and screening in free space, and overcome lossy media [32], [33]. The research on Vivaldi antennas that function at SWB frequencies using bandwidth-expanding approaches is still relatively restricted, particularly those that can cover the very low VSWR performance at all SWB frequencies.

However, interference is a serious problem at UWB and SWB frequencies because certain bands must notched out to avoid interference from other network technologies including Wifi and Wimax communications. Band-notch technique and Reconfigurable antennas have tunable characteristics including operating frequency, bandwidth impedance, and polarization are candidates to provide multifunctionality [34]. Many techniques have been carried out to block unwanted frequencies such as split-ring resonators, complementary split-ring resonators, open-loop resonators, and discrete filters [35], [36], [37]. The use of discrete filters is done by providing additional components thereby increasing the size of the antenna [38], [39]. It is necessary to research antennas that work UWB and SWB by examining notched bands for numerous frequencies that might create interference, as well as research on boosting antenna gain and polarization so that single antennas can be utilized for a variety of desired applications.

We investigate a novel compact Coplanar Vivaldi Antenna (CVA) with the same element width namely 5 cm ($0.39\lambda_L$) by varying the length of the antenna and the tapered slot. it produces a very wide bandwidth from 2,3 GHz to more than 30 GHz. The antenna has an S_{11} of less than -14 dB at all frequencies covering 2.4 to more than 30 GHz. There are seven different kinds of antennas: Coplanar Vivaldi Antenna Conventional (CVA-C) with the size 5×5 cm^2, CVA-LS (Long-Slot) and CVA-SS (Short-Slot) with the size 5×10 cm^2, also CVA-LS (Long-Slot) and CVA-LS (Short-Slot) and Wave Coplanar Vivaldi Antenna with/without CSRR (Complimentary split Ring Resonator) with the size 5×5 cm^2.

The SWB CVA antenna that we propose is created using the four step techniques outlined below and produces novelty:

1) Varying the length of the Vivaldi tapered slot to improve the bandwidth of the antenna. Presently, the most extensively produced Vivaldi antenna is the AVA type antenna since it has a broader bandwidth than CVA. Vivaldi antenna research typically has a fractional bandwidth that is not very broad, with a maximum S_{11} of roughly -10 dB. Typically, the bandwidth is increased by expanding the antenna, but no one has

investigated the effect of modifying the length of the tapered slot on the antenna bandwidth. We altered the length of the tapered slot, to create greater performance, specifically a very broad bandwidth (SWB frequency). We found that CVA-SS can work from frequency 2.3 to more than 30 GHz with a maximum S_{11} of −15 dB at these all frequency band and minimum S_{11} of −62.21 dB.

2) To boost the gain, the patch structure is modified using a wave structure. To improve the gain of the Vivaldi antenna, lenses/additional substrates, metamaterials, or a corrugated structure are typically added. We added a wavy structure on CVA and it received an increase in gain at most of the antenna's operating frequencies, with the highest increase in directivity occurring at the 15 GHz frequency of 5.77 dBi. (CVA-SS has a directivity of 2.35 dBi while WCVA-SS (using wave structure) has directivity 8.12 dBi at 15 GHz)
3) Add CSRR to see the notched-band frequencies. Currently, the notched band technique has been accomplished by adding extra external devices or constructing meanderline or parasitic structures that have a more sophisticated design and generally generate only several notched bands. Since Vivaldi antennas operate at such a wide frequency range, they may be interfered with by other wireless network technologies, we provide a Square CSRR structure on the opposite side of the feeder so that four notched-band frequencies are generated. In this study, the intended frequency of the notched-band may be altered by changing the position and geometry of the CSRR. The 3.33 - 3.72 GHz (WiMAX spectrum), 4.72 - 5.35 GHz (WLAN), 6.07 - 6.74 GHz (Wifi 6E use), and 7.40 - 8.29 GHz (X-satellite bands) are the constructed of our antenna notched bands.
4) Modify the CSRR patch to know the circular polarization. Typically, Vivaldi antennas have linear polarization, and there is currently very little study on single Vivaldi antennas that covers circular polarization. In this study, we arranged four CSRR in a U shape to create numerous frequencies with Axial Ratio values less than three, including the 4.6-5.3 GHz frequency, which has a minimum AR of 0.438, 7.8-8.2 GHz with min AR 0.732 and 26.92-27.7 GHz with min AR 2.13.

The following sections are presented in such an order: Section II details the configuration and parameters of the proposed antenna. Section III Result and Discussion, and a conclusion is drawn in Section IV.

II. CONFIGURATION AND PARAMETER OF THE ANTENNA

Figures 1 and 2 show the geometry and configuration of the SWB Coplanar Vivaldi Antenna (CVA). The antenna is designed on an FR4 epoxy substrate with a dielectric constant of 4.6, a thickness of 1.6 mm, and a loss tangent tan $\delta = 0.025$. The antenna's radiation patch, which is composed of copper

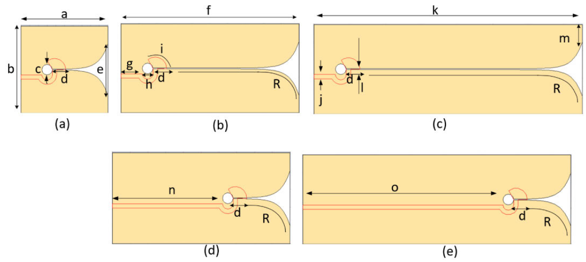

FIGURE 1. Coplanar Vivaldi Antenna (CVA): (a). 5 cm CVA-C (Conventional), (b) 10 cm CVA-LS (Long Slot), (c) 15 cm CVA-LS (d) 10 cm CVA-SS (Short Slot),and (d) 15 cm CVA- SS.

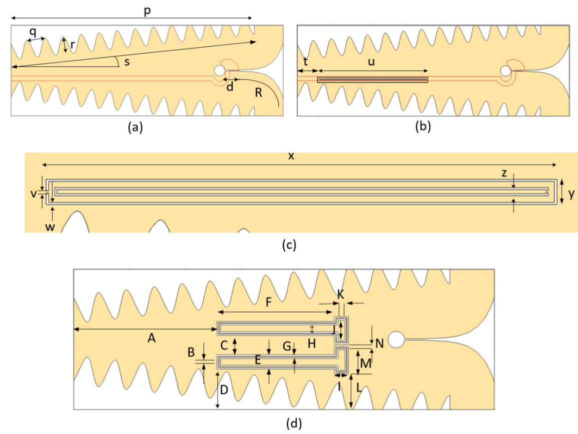

FIGURE 2. Wave Coplanar Vivaldi Antenna : (a) W-CVA, (b) W-CVA with Complementary split ring resonator(CSRR) and (c) CSSR and (d) variation U-shape 4 CSRR.

TABLE 1. Parameter dimension of the antenna.

Antenna dimension in mm					
Par	Dim	Par	Dim	Par	Dim
a	50	o	112	B	0.5
b	50	p	134	C	7
c	3	q	10	D	14.5
d	7.5	r	15	E	5
e	30	s	6^0	G	1.25
f	10	t	11	H	2.5
g	12	u	60.5	I	5
h	6	v	0.25	J	7.25
i	120^0	w	0.25	K	0.5
j	2.5	x	63	L	0.75
k	150	y	3	M	9.75
l	0.5	z	1	N	0.75
m	10	R	0.5		
n	62	A	51		

with 0.035 mm thickness, is mounted on the top and bottom of a printed circuit board (PCB).

Figure 1(a) shows a conventional Vivaldi coplanar antenna (CVA-C), while Figures 1 (b) and (d) are CVA antennas with a length of 10 cm but have different tapered slot lengths. Figure 1(b) is a Vivaldi antenna with a tapered slot length R which is longer than in Figure 1(d). The dimension of CVA-C is 50×50 × 1.6 mm^3 and it equal to $0.39\lambda_L \times 0{,}39\lambda_L \times 0{,}012\lambda_L$ (f_L=2.37 GHz). To describe the slope of the tapered slot, equation 1 can be used.

$$y = C_1.e^{Rx} + C_2, C_1 = \frac{y_2 - y_1}{e^{Rx_2} - e^{Rx_1}}, C_2 = \frac{y_1 e^{Rx_2} - y_2 e^{Rx_1}}{e^{Rx_2} - e^{Rx_1}} \tag{1}$$

In equation 1. y is the coordinate of the point which forms the slope of the tapered slot and its value is based on the constants C_1 and C_2. x_1, y_1 and x_2, y_2 are the start and end coordinates that will form the tapered slot line. We determine the initial center point of the x and y coordinates at the point (0,0) so that to form a tapered slot with an upward slope, the values (x_1, y_1) are (125, 25.25) and (x_2, y_2) has a value of (150, 40) while to form a tapered slot with a downward slope, the point (x_1, y_1) is (125,24.75) and (x_2, y_2) is (150,10). Points y_1, y_2 are determined based on the initial slot width (wsl) and the tapered slot opening width (wt).

In Figures 1 and 2, the entire antenna has the same fixed slot length d of 7.5 mm and after slotting d, the slot width will change according to the predetermined opening rate constant R. In this article, we set the value $R = 0.2$ for all coplanar tapered slots. The smaller the R-value, the wider the opening mouth between the two tapered slots. Figures 1(c) and (e) are CVA-LS (Long slot) and CVA-SS (Short Slot) with an antenna length of 15 cm. Figure 2(a) is a CVA-SS which has a wave structure on both edges of the antenna and in this case, we called it WCVA-SS. The wave structure follows equation 2, where we set the values of $K_1 = 2$, $K_2 = 1$, $K_3 = 2.5$, $K_4 = 2$ and $K_5 = 10$. By changing the K value, the length/width, depth, and number of waves will change the geometry following equation 2.

$$f(t) = K_1 \left(K_2 - K_3 \cos\left(\frac{K_4 \pi t}{K_5} \right) \right) \tag{2}$$

Figure 2(b) shows the WCVA-SS with CSRR structure. The CSRR structure is made up of two concentric rings with opposing opening orientations. A split-ring resonator's (SRR) complement image is called a CSRR. It is accomplished in a patch antenna by excising the copper shaped like an SRR from the ground plane of CVA as shown in Figure 3. Voltage gradients between the CSRR gap and inductance happen when the current flows along the CSRR coils. The effective permittivity in the vicinity of the resonant frequency is altered by the CSRR's ability to interact with the electric field. When an external magnetic flux is applied, the SRR can function as a magnetic dipole, and when an external electric field is applied, the CSRR can function as an electric dipole. The notch center frequency and the total size of the CSRR are correlated [40], [41]. The CSRR's whole perimeter as shown

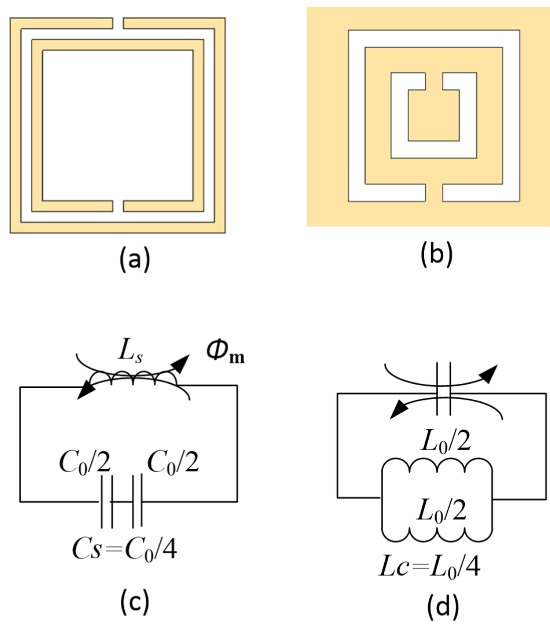

FIGURE 3. The structure model of an (a) SRR, (b). CSRR, (c) Equivalent circuit of SRR and (d) Equivalent circuit of SRR.

in equation (3)

$$L = \lambda/2 = \frac{c}{f_n \sqrt{\varepsilon_{eff}}} n = 1, 2, 3, ..\varepsilon_{eff} = \frac{\varepsilon_{er} + 1}{2} \tag{3}$$

where c is the speed of the light (3×10^8m/s), ε_{er} is dielectric constant of 4.6, ε_{eff} is the equivalent permittivity and where is the total length of the CSRR. The resonance frequency f_n of the CSRR can be set to get the notched band. To improve the stopband suppression effect, the two split rings' perimeters should be sufficiently close to one another.

An LC resonator can be used to model the SRR. The general equation for describing the analogous LC circuit for the SRR and CSRR circuits is in the Equation 4-8. The corresponding CSRR circuit that we utilize is shown in Figure 9, which is a simplified Chebyshev impedance matcher high order high pass filter. We used Qucsstudio software to obtain several resonant frequencies in the equivalent circuit that we created. Many steps of the tee type circuit coupled between C and L are required. The capacitance between the two rings, represented by C_0, is provided by equation (4)):

$$C_0 = 2\pi.dm.C_{pul} \tag{4}$$

where dm is the average length between the two rings and C_{pul} is the total capacitance between the rings per unit length. The value of dm is 0.75 mm. The SRR's rings' series capacitance and inductance are determined by equation (5):

$$C_s = C_0/4 \tag{5}$$

and the inductance of a single ring with length d can be used to estimate Ls. The SRR's resonance frequency is

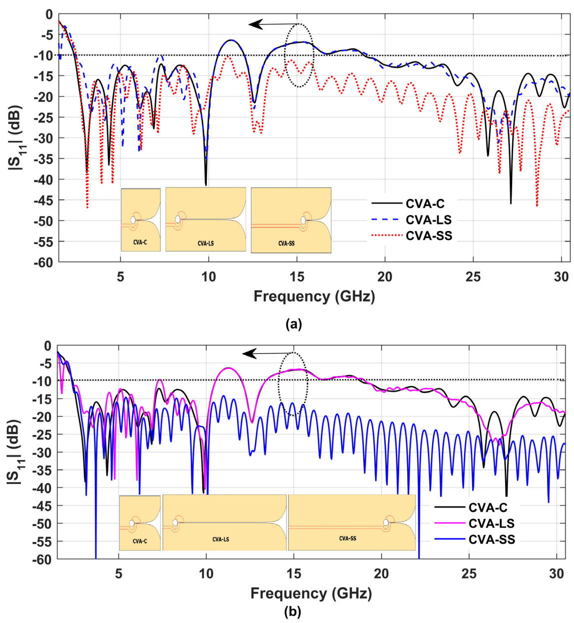

FIGURE 4. Return Loss performance of (a) 5 cm CVA-C, 10 cm CVA-LS, 10 cm CVA-SS and (b) 5 cm CVA-C, 15 cm CVA-LS, 15 cm CVA-SS.

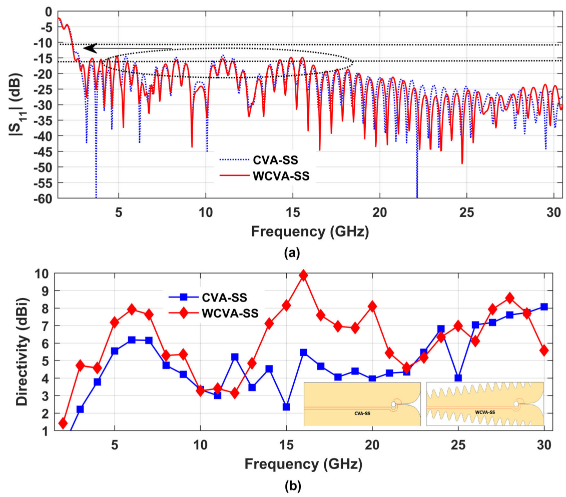

FIGURE 5. Return Loss performance of (a) 5 cm CVA-C, 10 cm CVA-LS, 10 cm CVA-SS and (b) 5 cm CVA-C, 15 cm CVA-LS, 15 cm CVA-SS.

determined by equation (6):

$$f_0 = \frac{1}{2\phi\sqrt{L_s C_s}} \tag{6}$$

As demonstrated in Figure 3, the CSRR may be represented as an LC resonator using the duality principle by substituting series capacitance for the shunt inductance and shunt inductors (equation (7)) for the series capacitors.

$$L_0 = 2\pi.d.L_{pul} \tag{7}$$

where the per-unit length inductance is denoted by Lpul. The CSRR's rings' series capacitance and inductance are determined by equation (8)

$$L_c = L_0/4 \tag{8}$$

III. RESULT AND DISCUSSION

From the simulation results in Figure 4, it is found that antennas CVA-C (5 cm in length), CVA-LS (10 cm in length), and CVA-SS(10 cm in length) have a S_{11} below -10 dB at the low-end frequencies are 2.37 GHz, 2.45 GHz, and 2.48 GHz. It can also be seen that the CVA-C and CVA-LS antennas have S_{11} above -10 dB at frequencies 10.53-12.02 GHz and 13.4-19.05 GHz, but for frequencies above 2.3 GHz apart from these frequencies, this antenna has S_{11} below -10 dB. The CVA-SS with the antenna length 10 cm and 15 cm has an S_{11} below -10 dB across all frequencies from 2.4 to more than 30 GHz. In this case, we just simulated the antenna until 30 GHz. We only simulate antennas up to 30 GHz to make the antenna performance graph clearer. However, we attempted to simulate up to 60 GHz (see Figure 6(a) and discovered that all S_{11} performance meets below -10 dB at frequencies 2.3 to greater than 60 GHz. Presently we utilize FR4 material in our simulation which is easy and cheap to find but is actually not suggested for high frequency usage. The wider the antenna bandwidth, it needs the more simulation time and the higher the computer specifications. According to the simulation findings, the S_{11} CVA-C and CVA-LS (Long SLot) with antenna lengths of 5 cm, 10 cm, and 15 cm exhibit comparable loss performance. At 11.39 GHz those antennas has maximum S_{11} is -6.5 dB and at 15.36 GHz the S_{11} maximum is -6.89dB. However At 11.39 GHz those antennas has maximum S_{11} is -6.5 dB and at 4.36 GHz the S_{11} maximum is -6.89dB. However at 11.09 GHz, the CVA-SS antenna with a length of 10 cm has a maximum S_{11} of -10.4 dB, whereas the antenna with a length of 15 cm has a maximum S_{11} of -14.3 dB.

Figure 5 shows the comparison of return loss and directivity between CVA-SS and WCVA-SS in 15 cm antenna length. It can be seen that both antennas have similar return loss performance. WCVA-SS antenna has a bandwidth from 2.31 GHz to more than 30 GHz resulting in S_{11} values below -15 dB at most frequencies. Antenna CVA-SS has the best return loss performance at 3.7 GHz and 22,15 GHz which is equal to -60.99 dB and -62.21 dB. Figure 5(b) shows that the directivity performance of the WCVA-SS antenna is better than the CVA-SS antenna without a wave structure at most frequencies. At the frequencies, 5 GHz, 6 GHz, 7 GHz, 14 GHz, 15 GHz, 16 GHz, 20 GHz, and 25 GHz the CVA-LS antenna has a directivity of 5.54 dBi, 6.17 dBi, 6.15 dBi, 4.52dBi, 2.35 dBi, 5.46 dBi, 3.96 dBi, and 4.00 dBi while the WCVA-SS has a directivity of 7.17 dBi, 7.92 dBi, 7.63 dBi, 7.18 dBi, 8.15 dBi, 9.86 dBi, 8.09 dBi, and 6.98 dBi. It means that the WCVA-SS results in increased gain of 1.63 dBi (5 GHz), 1.75 dBi (6 GHz), 1.48 dBi (7 GHz), 2.66 dBi (14 GHz), 5.8 dBi (15 GHz), 4.40 dBi (16 GHz), 3.90 dBi (20 GHz) and 2.98 dBi (25 GHz). By providing

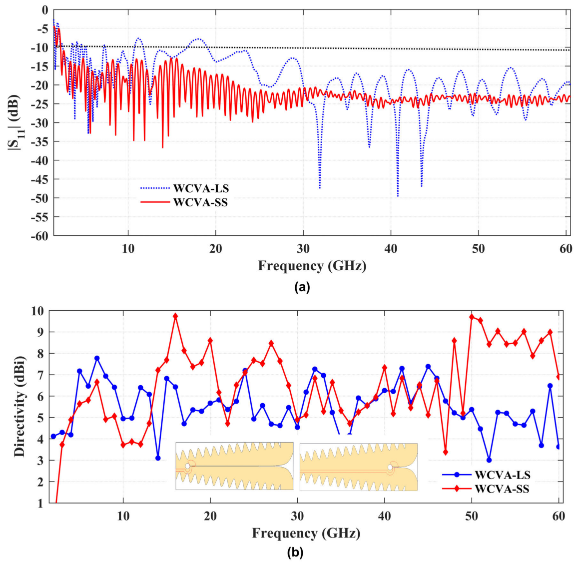

FIGURE 6. The performance of WCVA-LS and WCVA-SS in (a)Return Loss, (b) directivity vs freq.

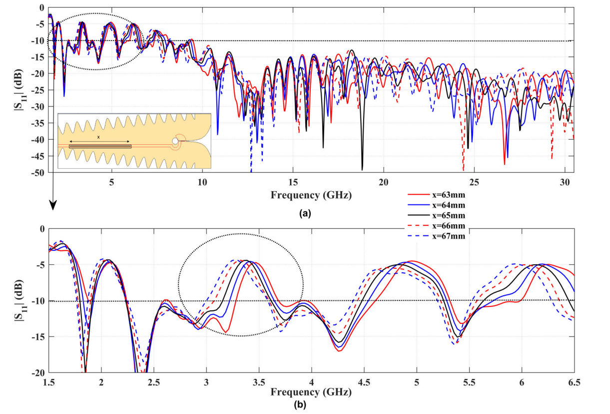

FIGURE 7. Return Loss performance of WCVA-SS with variation the length (x) of CSRR (a) at fequency 1.5-30 GHz and (b) the zoom out at a frequency of 1.5-7.5 GHz.

a wavy structure, the highest increasing gain occurred at the 15 GHz frequency of 5.8 dBi.

Meanwhile, Figure 6 is a comparison of return loss and gain between WCVA-LS and WCVA-SS from 2-60 GHz.In our simulations, we use CST. We carefully selected the material properties to model the FR4 substrate. CST allows for the selection of 'lossy' material models. For our study, we chose the 'lossy' material model to accurately represent the FR4 substrate, which includes its frequency-dependent permittivity and loss tangent. This approach ensures that our simulation results more closely reflect the real-world performance of the antenna, including the impact of dielectric losses at high frequencies. We acknowledge that the losses in FR4 increase with frequency, and our simulation settings were adjusted to take this into account, providing a realistic estimation of the antenna's performance up to 60 GHz. From Figure 6(a) it can be seen that all WCVA-SS return losses meet 10 dB, but for WCVA-LS there are several frequencies that have an S_{11} of more than -10 dB. From Figure 6(b), it can be seen that under 13 GHz WCVA-LS has better directivity performance than WCVA-SS. However, for frequencies above 13 GHz - 60 GHz, the directivity performance of WCVA-SS is better than WCVA-LS at most working frequencies.

Fig.7 displays the return loss performance of WCVA with a square-CSRR structure on the side opposite the feeding. According to the simulation results, increasing the CSRR size causes changes in return loss performance. Fig.7(a) shows that some S_{11} values are more than -10 dB for frequencies less than 9 GHz. Figure 7(b) shows that there are multiple repeating notched band frequencies. At a frequency of roughly 2 GHz, adding the S-CSRR structure results in an maximum S_{11} WCVA of -2.55 dB with the CSRR length of 63 mm. By using an S-CSRR structure, several notched bands are repeated at frequencies over 3 GHz. The notched frequency band of about 3 GHz changes towards a lower frequency (shifts to the left) when the x value increases. This can be seen that when = 63 mm the notched band occurs at a frequency of 3.28 - 3.68 GHz with a maximum S_{11} of -4.7 dB (3.48 GHz), while for x = 67 mm, the notched band occurs at a frequency of 3.00 - 3.58 GHz with a maximum S_{11} of -4.4 dB (3.29 GHz). The notched band will repeat at numerous frequencies. In this case, the notch band frequency may be adjusted by modifying the CSRR length based on equation 9.

$$f_c = 1.45.\frac{c}{L\sqrt{\varepsilon_{eff}}} \quad (9)$$

Figure 8 depicts S_{11} 's performance when the width of the S-CSRR is varied. The larger the width of S-CSRR, the lower the low-end frequency and it shifts to roughly 3 GHz. It can be shown that the low-end frequency at S_{11} -10dB for y = 6 mm, 5 mm, 4 mm, 3 mm, and 2 mm is 2.922 GHz, 3.02 GHz, 3.133 GHz, 3.324 GHz, and 3.505 GHz. Meanwhile, the high-end frequencies for y = 2 mm, 3 mm, 4 mm, 5 mm, and 6 mm are 3.723 GHz, 3.781 GHz, 3.988 GHz, 4.218 GHz, and 4.26 GHz, respectively. Based on the current data, the broader the S-CSRR, the greater the bandwidth in the notched band frequency. This may be observed for y = 6 cm, 5 mm, 4 mm, 3 mm, and 2 mm with notched band bandwidths of 1.338GHz, 1.192GHz, 0.855GHz, 0.457GHz, and 0.218GHz. The Notched frequency band is broadest at y=6 cm and smallest at y=2 cm. However, the highest S_{11} value occurs for y = 6 mm and the maximum S_{11} for y = 2cm.

To investigate the wideband characteristics of ultra-wideband antennas, an equivalent circuit model of WCVA-SS was created in the Qucsstudio 4.3.1 (Quite Universal Circuit Simulator) like an ADS simulator, as shown in Fig. 9(a) without CSRR and Fig.(b) with CSRR, while Fig 9(c) demonstrates the return loss performance and its comparison between Qucsstudio and EM simulation result. By using a

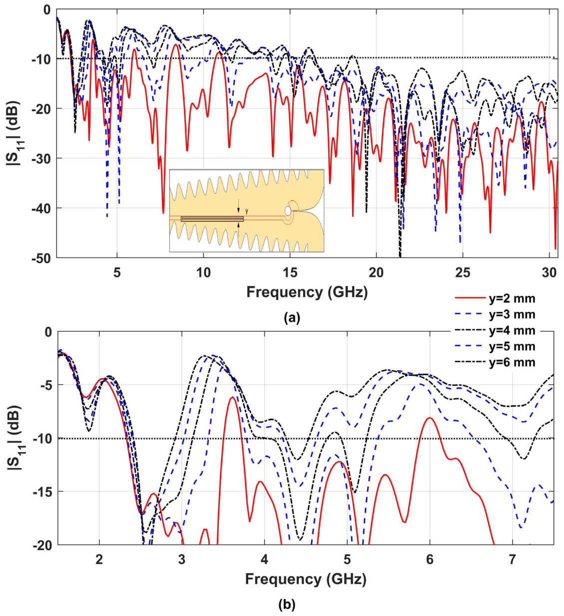

FIGURE 8. Return Loss performance of WCVA-SS with a variation in the width (y): (a) at frequency 1.5-30 GHz and (b) the zoom out at a frequency of 1.5-7.5 GHz.

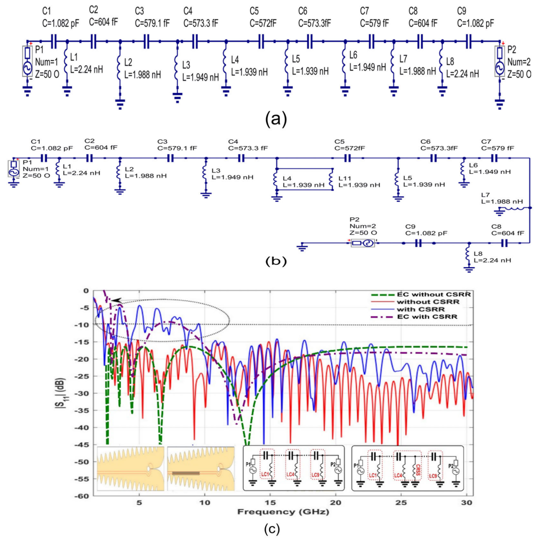

FIGURE 9. The Return Loss performance of WCVA-SS (a) without CSRR, (b) with Square-CSRR and (c) the comparison of return loss performance.

Square-CSRR construction, it can give numerous notched band frequencies at frequencies less than 9 GHz. It raises numerous S_{11} levels at different frequencies. The WCVA, as it is a Vivaldi type antenna, is by nature UWB, which guarantees adequate matching between the characteristic impedance of the feed Z_0 of the 50 Ohm with the intrinsic impedance of the free space, Z_{air} of the 377 ohm in a wide frequency range, in this case, the equivalent circuit(EC) can be simplified to a Chebyshev network impedance matcher, as a high-order high-pass filter, as can be seen in the illustration of the equivalent circuit in Figure 9 with nine LC-type resonant elements. CRSS adds an equivalent inductance to LC element number 4 of the network, which moves the lower frequency limit (cutoff frequency in the case of the equivalent circuit) to 9.75GHz.. Simulation result shows the four notched bands developed at frequencies 3.335 - 3.72 GHz (IEEE 802.16 WiMAX spectrum) [42], 4.72 - 5.354 GHz (IEEE 802.11a WLAN), 6.07 - 6.743 GHz (Wifi 6E use), and 7.408 - 8.293 GHz (X-band satellite uplink and downlink communication) with maximum S_{11} of -4.914 dB, -4.366 dB, -5.2 dB, and $-7{,}625$ dB. More study is required to verify that the notch band created has a greater maximum S_{11} by making the frequency filtering more reliable/sharp. By modifying the position, length, and width of the S-CSRR, the notched band frequency may be further adjusted to prevent interference at numerous narrow microwave frequencies.

The directivity performance between CVA-C (5 cm), CVA-LS (10 cm), and CVA-SS (10 cm) can be seen in Figure 10(a). At 5 GHz, the directivity values are 4.2 dBi, 4,667 dBi, and 5,498 dBi (CVA-C, CVA-LS, and CVA-SS), respectively. At 15 GHz, the directivity values are 2,056 dBi, 2,343 dBi, and 3,714 dBi ((CVA-C (5 cm), CVA-LS (10 cm), and CVA-SS (10 cm)). Even though the return loss performance data suggest that CVA-SS has the widest bandwidth, as shown in Figure 4(a), this can be interpreted as an unstable increase and reduction in gain. Figure 10(b) shows the difference in directivity between CVA-C (5cm) and CVA-LS (15 cm), CVA-SS (15 cm), and WCVA-SS (15cm). It can be shown that at 5 GHz, the directivity created is 4.2 dBi, 4.61 dBi, 5.549 dBi and 7.172 dBi for CVA-C (5cm), CVA-LS, CVA-SS, and WCVA-SS with the antenna length 15 cm. Whereas at the 15 GHz frequency the directivity formed is 2.057dBi, 2.355dBi, 2.658 dBi and 8.125dBi acquired for CVA-C, CVA-SS, CVA-LS and WCVA-SS. It can be observed that the directivity values of CVA without a wave structure are relatively similar at this frequency. however the WCVA-SS has a directivity improvement of 5.77 dBi when compared to CVA-SS without a wave structure. When compared to CVA-LS, at 16 GHz WCVA-SS produces the maximum directivity of 9,865 dBi and a gain improvement of 4,785 dBi. WCVA-SS outperforms CVA without a wave structure at nearly all frequencies. The antenna's directivity can be enhanced by incorporating a corrugated construction since the electric field is focused in the corrugated structure.

Figure 11 depicts the variations in the polar form of radiation patterns for frequencies of 3 GHz, 5 GHz, 8 GHz and 12GHz at θ 90^0. While Figure 12 shows the polar plot radiation pattern at 16 GHz, 22 GHz, 28 GHz and the directivity vs frequency between WCVA without and with CSRR. At the 3 GHz frequency, WCVA has a major lobe of 4.71 dBi, main lobe direction of 349^0, angle width of 52.3^0, and side lobe level -0.5 dB whereas CSRR-WCVA has a main lobe direction of 3.7 dBi, main lobe direction of 351.0^0, angular width(3dB) of 52.4^0 and sidelobe level

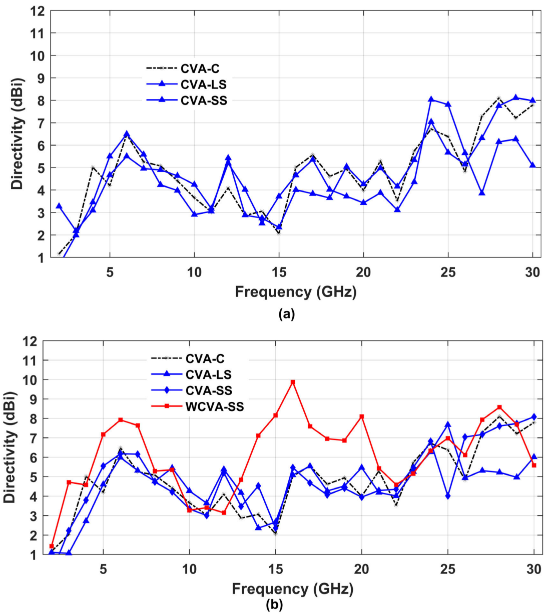

FIGURE 10. Directivity of Coplanar Vivaldi Antenna (a) CVA-C (5 cm), CVA-LS (10 cm), CVA- SS 10 cm(15cm) dan (b) CVA-C (5cm), CVA-LS(15cm), CVA-SS(15cm) dan WCVA-SS (15cm).

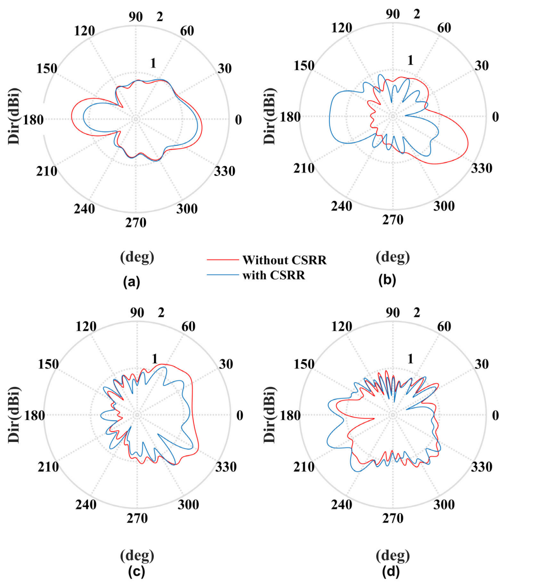

FIGURE 11. Polar plot of radiation pattern WCVA with/without CSRR at (a) 3 GHz, (b) 5GHz, (c) 8 GHz and (d) 12GHz.

−2.2 dB. At 3 GHz, WCVA without CSRR has stronger directivity than WCVA with CSRR, while the converse is true for the side lobe level. At 5 GHz, WCVA without CSRR has a gain of 7.18 dBi and a sidelobe level of −7.7 dB, whereas WCVA with CSRR has a gain of 4.09 dBi and a sidelobe level of −2.4 dB. At 5 GHz, the difference in directivity and sidelobe levels is 3.09 dBi and 5.3 dBi, respectively. At 8 GHz, the WCVA has a gain of 5.3 dBi, an angular width of 53.8^0, and a sidelobe level of −1 dB, whereas a WCVA with CSRR has a main lobe magnitude of 4.16 dBi,

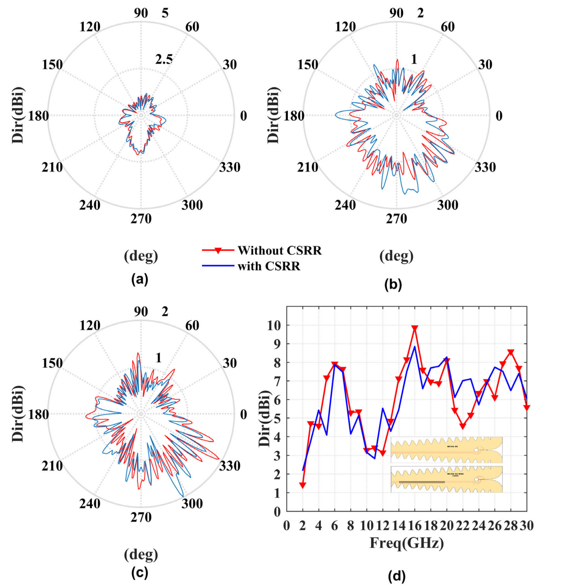

FIGURE 12. Polar plot of radiation pattern WCVA with/without CSRR at (a)16 GHz, (b) 22GHz and (c)28 GHz and the performance of directivity vs freq.

an angular width (3 dB) 16.6^0, and a sidelobe level of −1.7 dB. At 8 GHz, there is only a 1.14 dBi significant difference in directivity and side lobe level for both WCVA without and with CSRR. Figure 12(a)-(c) represents the antenna radiation pattern at frequencies 16 GHz, 22 GHz, and 28 GHz, whereas Figure 12(d) displays the directivity performance in relation to frequency. At 22 GHz, the WCVA with CSRR has a directivity of 7.00 dBi, whereas without it it has a directivity of 4.58 dBi. At 28 GHz, the gain of the WCVA with CSRR is 6.48 dBi, whereas the gain of the WCVA without CSRR is 8.57 dBi. By using a CSRR structure at 22 GHz, no band-notching occurs, resulting in no drop in gain. Providing a CSRR structure at the 22 GHz frequency boosts antenna gain by 2.42 dBi over not having one. Using CSRR at 28 GHz results in a band-notched frequency, lowering the gain by 2.09 dB. It is expected that utilizing a CSRR construction will result in band-notched at the target frequency, resulting in a decrease in antenna gain, indicating that the antenna is not working optimally. The directivity of an antenna without CSRR is higher than that of an antenna with CSRR at frequencies of 3 GHz, 5 GHz, 8 GHz, 14-17 GHz, and 28 GHz. Because the antenna has an S_{11} greater than −10 dB, the existence of bandnotched results in a drop in radiation pattern performance, and vice versa.

Figure 13 depicts the difference in surface current between WCVA with and without CSRR. At 5 GHz, the surface current of WCVA with CSRR has more density that is concentrated in the CSRR structure (see Figure 13(b), resulting in notched bands at many frequencies. This demonstrates that the electric field is contained within the CSRR structure rather than being created externally. Meanwhile, in Figure 13(a), the surface current concentration is localized

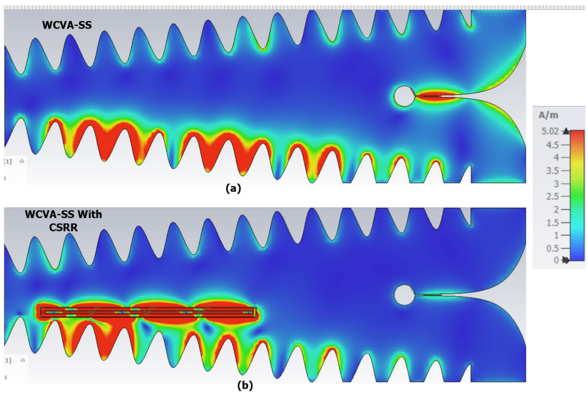

FIGURE 13. Surface Current at 5 GHz (a) WCVA-SS without CSRR and (b) WCVA with CSRR.

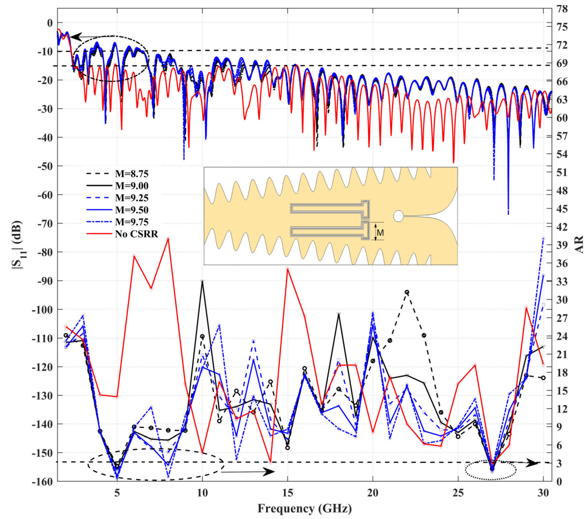

FIGURE 14. The comparison of WCVA-SS performance with M length variation in (a). Return loss performance, (b) AR performance.

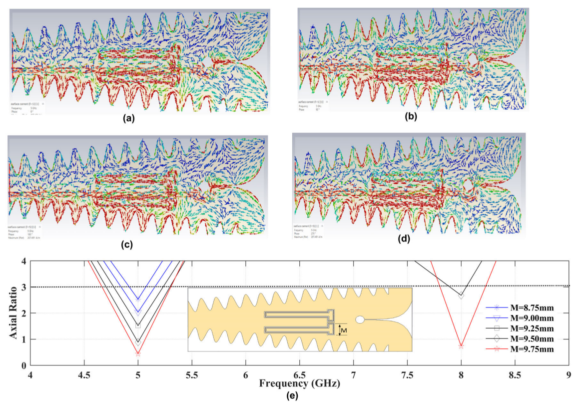

FIGURE 15. The comparison of surface current distribusion in different phase of: (a) 0 deg, (b) 90 deg, (c) 180 deg, (d) 270 deg) (e) the AR vs freq.

between the apertures of the two tapered slots that arround the circular cavity geometry. This demonstrates that the gain of this antenna at the 5 GHz frequency without CSRR is larger than the gain with CSRR.

The investigation of circular polarization on the WCVA antenna element can begin by supplying four CSRR structures with a U shape orientation, as illustrated in Figure 2(d), and the performance as shown in Figure 14 and 15. Figure 2(d) shows that the CSRR employed comprises of two vertical and two horizontal CSRRs. The horizontal CSRR is connected to the vertical, and the length and width of the CSRR position influence polarization performance. Figure 14(a) depicts the return loss performance of a WCVA antenna with a CSRR configuration in a U shape, with numerous notched band frequencies visible. Figure 14(b) and 15(e) demonstrate that AR 3 dB occurs across the frequency range 4.6-5.3 GHz, with a minimum AR of 0.438. Aside from that, AR 3 dB occurs at the 8 GHz frequency, which occurs in the 7.8 - 8.2 GHz frequency with a minimum AR of 0.732. Surface current at the 5 GHz frequency can be seen in Figure 15. It can be seen that the current density is concentrated more around the bottom CSRR (shown in red) and the direction of surface current movement is circular because it is blocked by the CSRR structure.

Modifications in the vertical length (M) of the CSRR have an impact on AR performance, as well as the CSRR's horizontal position and placement. More research is needed to enhance the AR bandwidth while maintaining the antenna's $S_{11} < -10$ dB value. Figure 15 depicts the surface current distribution on the WCVA-SS with circular polarization for various phases 0^0,90^0,18^0, and 270^0 degrees, conveying the vector rotation. Figure 15 (a) and (c) show that the rotation vector for phase 0^0 is opposed to phase 180^0, However the rotation vector for phase 90^0 is contrary to phase 270^0. Circular polarization is created by using a U-shaped CSRR structure. It is possible to build a circular polarization of WCVA antenna by altering the CSRR slot.

Figure 16 depicts a comparison between simulation results with S_{11} WCVA measurements taken with the Keysight VNA. At most frequencies, notably below 10 GHz, there is a good agreement between simulation and measurement. Even though some measurement results are slightly different from simulation results at high frequencies, this can be assigned to the specifications of the connectors and cables used a little improper for high frequencies up to 30 GHz. But overall it shows that the simulation and measurement results of WCVA seem good enough and good agreement because all of the measurement result cover S_{11} below -10dB from 2,3 Ghz until 30 GHz and indicating that this antenna can be used for a variety of applications.

Table 2 compares the WCVA-SS antenna with related references in terms of similarity of broadband, UWB, and SWB antennas and band notched techniques. In this comparison, we utilize a monopole antenna [31], [33], bowtie [54], Dipole [55] and a Vivaldi antenna [43], [44], [45], [46], [47], [48], [49], [50], [51], [52], [53], [56] since both can typically span broadband frequencies. Despite its tiny size, the antenna [31] only operates at the UWB frequency

TABLE 2. Comparison with other related referenced.

Ref Ant. Type	Ant. size(mm^2) Subs, Method/type	Freq(GHz) 10dB% BW	Notched band (GHz)
[31] Monopole	$0.37\lambda_L \times 0.37\lambda_L$ FR4, Slit	3.1 - 10.6 109	5.15-5.58
[33] Monopole	$0.16\lambda_L \times 0.37\lambda_L$ FR4,Fractal	1.44-18.8 172	N.A
[43] BAVA	$1.12\lambda_L \times 2.1\lambda_L$ RT5880, UWB	6-20 108	N.A
[44] AVA	$1.2\lambda_L \times 1.2\lambda_L$ RO 04003,MPSO	3-11 114	N.A
[45] AVA	$4\lambda_L \times 4.92\lambda_L$ FR4, Radar	4 - 6.8 52	N.A
[46] AVA	$0.33\lambda_L \times 0.04\lambda_L$ FR4, Broadband	1-6 143	N.A
[47] AVA	$0.42\lambda_L \times 0.61\lambda_L$ FR4,Metamaterial	1.3 - 12 161	N.A
[48] AVA	$0.45\lambda_L \times 0.38\lambda_L$ FR4 sun slot,SRR Metalic via	1.1 - 14 171	2.2-2.7 3.3-3.6 4.7-5.6 8.8-9.5
[49] AVA	$0.66\lambda_L \times 0.66\lambda_L$ RO 4003 , EBG	3 - 11 114	3.6-3.9 5.6-5.8
[50] CVA	$0.44\lambda_L \times 0.54\lambda_L$ Open step impedance	1.88 - 12.1 146	3.6-3.9 4.9-6.6
[51] CVA	$0.71\lambda_L \times 0.92\lambda_L$ RO 4350, parasitic	6.75-16.15 82	13.7-15.4
[52] CVA	$0.25\lambda_L \times 0.25\lambda_L$ Tachonic, SRR	2.9-11.6 120	5.3-5.8 7.85-8.55
[53] CVA	$0.06\lambda_L \times 0.07\lambda_L$ FR4,Pin dioda Meanderline	0.45-4.5 164	0.45-0.85 5.1-5.8 3,3-3.8
[54] Ver Bowtie	$0.25\lambda_L \times 0.2\lambda_L$ FR4	3.00-17.39 141	NA
[55] Dipole	$0.69\lambda_L \times 0.69\lambda_L$ Tachonic RF35	3.2-9.6 100	5.1-5.4 5.6-5.9
[56] AVA	$0.41\lambda_L \times 0.9\lambda_L$ Rogers 4350B, Lens	22,5-45 67	NA
Our purpose CVA	$0.38\lambda_L \times 1.15\lambda_L$ FR4 Wave, CSRR	2.31 - 60 185	3.3-3.7 4.7-5.3 6-6.7 7.4-8.2

and creates one notched band, whereas the antenna [33] operates at a maximum frequency of 18.8 GHz and does not mention the notched band. The antenna mentioned in reference [43] is the BAVA antenna, which operates at a UWB frequency of 6-10 GHz. The BAVA antenna has two layers of substrate, whereas our antenna only has one layer of substrate and operates at lower low-end frequencies than this BAVA antenna. The antenna [43] is wider than our antenna, made of RO04003, and only operates at UWB frequencies, whereas our antenna works at SWB frequencies. References [44], [45], and [46] have similarly big dimensions and only work at frequencies UWB, 4-6.8 GHz and 1-6 GHz

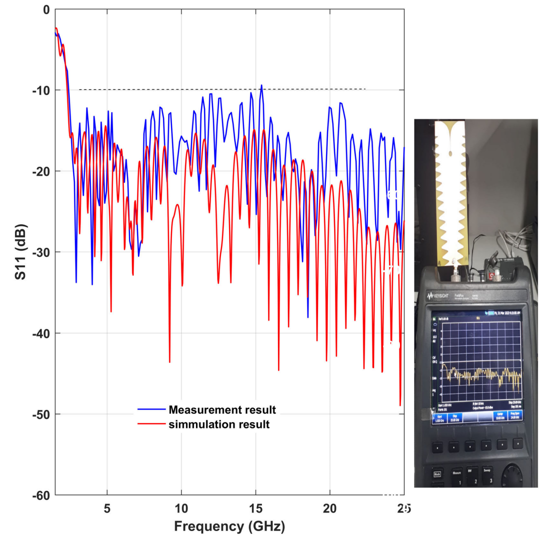

FIGURE 16. The comparison of Return loss performance from simulation and measurement results of WCVA.

using FR4 material. The antenna in reference [47] is an AVA antenna that employs metamaterial methods. It has broader antenna width than the antenna we constructed, and it does not mention the notched bands. Meanwhile, the antenna [48] has a bigger antenna width and employs a sun-shaped slot, SRR, and metal via, making the approach employed more complicated than the one we used, and it only runs at 1.1-14 GHz. Despite [49], [50] has diminutive size, but the antennas only function at UWB frequencies and feature two notched bands. Antennas [51] and [52] employ the same CVA antenna as the one we built, but they work at a little lower bandwidth than our purpose antenna and also create only 1 and 2 band-notched antennas. The antenna [53] uses meanderline techniques in feeding and PIN diodes, so there are additional external components and only operated at 0.4-12 GHz. Antenna [54], [55], [56] has the smaller bandwidth than WCVA. Whereas our purposes antenna produces 4-band-notched using a simple structure, namely CSRR-WCVA and can operated from 2.3 to more than 60 GHz.

IV. CONCLUSION

Coplanar Vivaldi antenna design have been carried out, namely CVA-C (5cm in length), CVA-LS (10 and 15cm in length), CVA-SS (10 and 15cm in length), WCVA-SS (15 cm in length) with and without CSRR. The CVA SS that has shorter tapered slot length has better bandwidth performance than the CVA-LS. The WCVA has S_{11} below -15 dB in all frequency work from 2.3 GHz to more than 30 GHz. CVA-SS has the best S_{11} at 22.15 GHz of -62.21 dB. By providing a wavy structure, the antenna gain performance can be increased in almost all frequency ranges An increase in gain of 5.8 dBi occurs at the 15 GHz frequency. By providing a CSRR structure, the antenna can block frequencies 3.3-3.7 GHz (IEEE 802.16 WIMAX band), 5-5.3 GHz (IEEE 802.11a WLAN and 6.1-6.8 GHz (Wifi 6E/ the sixth generation of Wifi 5.9-7.1). By providing a U-shaped configuration for 4 CSRR on the WCVA, it produces circular polarization on a single WCVA antenna at a frequency of 4.6-5.3 GHz with a minimum AR of 0.438. The WCVA antenna with a CSRR structure has the advantage of being able to work in SWB, having high gain, having notched bands at certain frequencies, and having circular polarization, allowing this single WCVA antenna to be used for a variety of telecommunications and radar technology applications.

REFERENCES

[1] A. M. Abbosh and M. E. Bialkowski, "Design of UWB planar band-notched antenna using parasitic elements," *IEEE Trans. Antennas Propag.*, vol. 57, no. 3, pp. 796–799, Mar. 2009, doi: 10.1109/TAP.2009.2013449.

[2] G. Hendrantoro, T. Fukusako, and E. Setijadi, "Mutual coupling reduction for a UWB coplanar Vivaldi array by a truncated and corrugated slot," *IEEE Antennas Wireless Propag. Lett.*, vol. 17, no. 12, pp. 2284–2288, Dec. 2018, doi: 10.1109/LAWP.2018.2873115.

[3] C.-H. Lee, J.-H. Wu, C. G. Hsu, H.-L. Chan, and H.-H. Chen, "Balanced band-notched UWB filtering circular patch antenna with common-mode suppression," *IEEE Antennas Wireless Propag. Lett.*, vol. 16, pp. 2812–2815, 2017, doi: 10.1109/LAWP.2017.2748279.

[4] S. Park and K.-Y. Jung, "Novel compact UWB planar monopole antenna using a ribbon-shaped slot," *IEEE Access*, vol. 10, pp. 61951–61959, 2022, doi: 10.1109/ACCESS.2022.3182443.

[5] M. Moosazadeh, S. Kharkovsky, J. T. Case, and B. Samali, "Miniaturized UWB antipodal Vivaldi antenna and its application for detection of void inside concrete specimens," *IEEE Antennas Wireless Propag. Lett.*, vol. 16, pp. 1317–1320, 2017, doi: 10.1109/LAWP.2016.2633536.

[6] A. Benouakta, F. Ferrero, L. Lizzi, and R. Staraj, "Antenna characteristics contributions to the improvement of UWB real-time locating systems' reading range and multipath mitigation," *IEEE Access*, vol. 11, pp. 71449–71458, 2023, doi: 10.1109/ACCESS.2023.3294622.

[7] P. Nergis and M. Moghaddam, "Compact dual-polarized UWB antenna for UAV based low-frequency software defined radar," in *Proc. IEEE Int. Symp. Antennas Propag. USNC-URSI Radio Sci. Meeting (AP-S/URSI)*, Jul. 2022, pp. 1796–1797, doi: 10.1109/AP-S/USNC-URSI47032.2022.9887158.

[8] C. M. Dikmen, S. Çimen, and G. Çakir, "Planar octagonal-shaped UWB antenna with reduced radar cross section," *IEEE Trans. Antennas Propag.*, vol. 62, no. 6, pp. 2946–2953, Jun. 2014, doi: 10.1109/TAP.2014.2313855.

[9] U. R. Khan, J. A. Sheikh, A. Junaid, R. Amin, S. Ashraf, and S. Ahmed, "Design of a compact hybrid Moore's fractal inspired wearable antenna for IoT enabled bio-telemetry in diagnostic health monitoring system," *IEEE Access*, vol. 10, pp. 116129–116140, 2022, doi: 10.1109/ACCESS.2022.3219442.

[10] M. E. de Cos Gómez, H. F. Álvarez, A. F. Berdasco, and F. Las-Heras, "Ultra-thin compact eco-friendly textile antenna for IoT: Zigbee application example," in *Proc. IEEE Int. Symp. Antennas Propag. North Amer. Radio Sci. Meeting*, Jul. 2020, pp. 1329–1330, doi: 10.1109/IEEECONF35879.2020.9330423.

[11] C. F. M. Carobbi, "A lumped model of the rod antenna setup adopted for military and automotive testing," *IEEE Trans. Electromagn. Compat.*, vol. 61, no. 4, pp. 1289–1296, Aug. 2019, doi: 10.1109/TEMC.2019.2902628.

[12] M. Ayyappan and P. Patel, "On design of a triple elliptical super wideband antenna for 5G applications," *IEEE Access*, vol. 10, pp. 76031–76043, 2022, doi: 10.1109/ACCESS.2022.3185241.

[13] P. Kumar, S. Urooj, and A. Malibari, "Design and implementation of quad-element super-wideband MIMO antenna for IoT applications," *IEEE Access*, vol. 8, pp. 226697–226704, 2020, doi: 10.1109/ACCESS.2020.3045534.

[14] A. Sabban, "Small new wearable antennas for IoT, medical and sport applications," in *Proc. 13th Eur. Conf. Antennas Propag. (EuCAP)*, Mar. 2019, pp. 1–5.

[15] B. Biswas, R. Ghatak, and D. R. Poddar, "A fern fractal leaf inspired wideband antipodal Vivaldi antenna for microwave imaging system," *IEEE Trans. Antennas Propag.*, vol. 65, no. 11, pp. 6126–6129, Nov. 2017.

[16] P. A. Dzagbletey, J.-Y. Shim, and J.-Y. Chung, "Quarter-wave balun fed Vivaldi antenna pair for V2X communication measurement," *IEEE Trans. Antennas Propag.*, vol. 67, no. 3, pp. 1957–1962, Mar. 2019, doi: 10.1109/TAP.2019.2893201.

[17] Z. Yin, G. He, X.-X. Yang, and S. Gao, "Miniaturized ultrawideband half-mode Vivaldi antenna based on mirror image theory," *IEEE Antennas Wireless Propag. Lett.*, vol. 19, no. 4, pp. 695–699, Apr. 2020, doi: 10.1109/LAWP.2020.2977503.

[18] L. Sang, J. Xu, Z. Liu, Y. Mei, W. Wang, and Z. Shen, "Low-RCS UWB planar monopole array antenna based on the optimized design of the conductor layers," *IEEE Trans. Antennas Propag.*, vol. 71, no. 4, pp. 3683–3688, Apr. 2023, doi: 10.1109/TAP.2023.3247905.

[19] M. Koohestani, N. Azadi-Tinat, and A. K. Skrivervik, "Compact slit-loaded ACS-fed monopole antenna for Bluetooth and UWB systems with WLAN band-stop capability," *IEEE Access*, vol. 11, pp. 7540–7550, 2023, doi: 10.1109/ACCESS.2023.3238577.

[20] F. M. Alnahwi, Y. I. A. Al-Yasir, N. T. Ali, I. Gharbia, C. H. See, and R. A. Abd-Alhameed, "A compact wideband circularly polarized planar monopole antenna with axial ratio bandwidth entirely encompassing the antenna bandwidth," *IEEE Access*, vol. 10, pp. 81828–81835, 2022, doi: 10.1109/ACCESS.2022.3196610.

[21] L. Sang, S. Wu, G. Liu, J. Wang, and W. Huang, "High-gain UWB Vivaldi antenna loaded with reconfigurable 3-D phase adjusting unit lens," *IEEE Antennas Wireless Propag. Lett.*, vol. 19, no. 2, pp. 322–326, Feb. 2020, doi: 10.1109/LAWP.2019.2961393.

[22] J. Eichenberger, E. Yetisir, and N. Ghalichechian, "High-gain antipodal Vivaldi antenna with pseudoelement and notched tapered slot operating at (2.5 to 57) GHz," *IEEE Trans. Antennas Propag.*, vol. 67, no. 7, pp. 4357–4366, Jul. 2019, doi: 10.1109/TAP.2019.2906008.

[23] M. Singh and M. S. Parihar, "Gain improvement of Vivaldi MIMO antenna with pattern diversity using bi-axial anisotropic metasurface for millimeter-wave band application," *IEEE Antennas Wireless Propag. Lett.*, vol. 22, no. 3, pp. 621–625, Mar. 2023, doi: 10.1109/LAWP.2022.3220710.

[24] J. Puskely, J. Lacik, Z. Raida, and H. Arthaber, "High-gain dielectric-loaded Vivaldi antenna for K_a -Band applications," *IEEE Antennas Wireless Propag. Lett.*, vol. 15, pp. 2004–2007, 2016, doi: 10.1109/LAWP.2016.2550658.

[25] J. Liu, H. Zhang, and J. Liu, "A 4-layer dielectric slab covered high-gain modified antipodal Vivaldi antenna," in *Proc. Cross Strait Radio Sci. Wireless Technol. Conf. (CSRSWTC)*, Dec. 2022, pp. 1–3, doi: 10.1109/CSRSWTC56224.2022.10098336.

[26] S. Ullah, A. R. Mashal, F. Hafeez, M. Alibakhshikenari, F. Arpanaei, B. S. Virdee, and F. Falcone, "Super-wideband antenna with multiple notched-band functionality through L-X bands," in *Proc. Asia–Pacific Microwave Conf. (APMC)*, Nov. 2022, pp. 860–862, doi: 10.23919/apmc55665.2022.9999851.

[27] A. K. Chaudhary and M. Manohar, "A modified SWB hexagonal fractal spatial diversity antenna with high isolation using meander line approach," *IEEE Access*, vol. 10, pp. 10238–10250, 2022, doi: 10.1109/ACCESS.2022.3144850.

[28] D. Tran, V. Paraforou, and A. Yarovoy, "A novel 1-decade super wideband UHF antenna for GPR and impulse radio applications," in *Proc. 8th Eur. Conf. Antennas Propag. (EuCAP)*, Apr. 2014, pp. 3073–3077, doi: 10.1109/EuCAP.2014.6902476.

[29] W. Balani, M. Sarvagya, T. Ali, M. Pai M. M., J. Anguera, A. Andujar, and S. Das, "Design techniques of super-wideband antenna–existing and future prospective," *IEEE Access*, vol. 7, pp. 141241–141257, 2019, doi: 10.1109/ACCESS.2019.2943655.

[30] C. Yu, S. Yang, Y. Chen, W. Wang, L. Zhang, B. Li, and L. Wang, "A super-wideband and high isolation MIMO antenna system using a windmill-shaped decoupling structure," *IEEE Access*, vol. 8, pp. 115767–115777, 2020, doi: 10.1109/ACCESS.2020.3004396.

[31] H. Zhao, F.-S. Zhang, X.-K. Zhang, and C. Wang, "A compact band-notched ultra-wideband spatial diversity antenna," *Prog. Electromagn. Res. C*, vol. 51, pp. 19–26, 2014, doi: 10.2528/PIERC14042101.

[32] H. Ullah, S. U. Rahman, Q. Cao, I. Khan, and H. Ullah, "Design of SWB MIMO antenna with extremely wideband isolation," *Electronics*, vol. 9, no. 1, p. 194, Jan. 2020, doi: 10.3390/electronics9010194.

[33] K.-R. Chen, C.-Y.-D. Sim, and J.-S. Row, "A compact monopole antenna for super wideband applications," *IEEE Antennas Wireless Propag. Lett.*, vol. 10, pp. 488–491, 2011, doi: 10.1109/LAWP.2011.2157071.

[34] H. Boudaghi, M. Azarmanesh, and M. Mehranpour, "A frequency-reconfigurable monopole antenna using switchable slotted ground structure," *IEEE Antennas Wireless Propag. Lett.*, vol. 11, pp. 655–658, 2012, doi: 10.1109/LAWP.2012.2204030.

[35] K. Sathish, C. Saha, D. Sarkar, J. Y. Siddiqui, and Y. M. M. Antar, "Varactor-controlled SRR-integrated frequency-reconfigurable multifunctional Vivaldi antenna: A proposed concept," *IEEE Antennas Propag. Mag.*, vol. 64, no. 3, pp. 82–94, Jun. 2022, doi: 10.1109/MAP.2021.3106893.

[36] C. Feng, T. Shi, and L. Wang, "Novel broadband bow-tie antenna based on complementary split-ring resonators enhanced substrate-integrated waveguide," *IEEE Access*, vol. 7, pp. 12397–12404, 2019, doi: 10.1109/ACCESS.2019.2893881.

[37] A. Salim and S. Lim, "Complementary split-ring resonator-loaded microfluidic ethanol chemical sensor," *Sensors*, vol. 16, no. 11, p. 1802, Oct. 2016, doi: 10.3390/s16111802.

[38] G.-P. Gao, B.-K. Zhang, J.-H. Dong, Z.-H. Dou, Z.-Q. Yu, and B. Hu, "A compact dual-mode pattern-reconfigurable wearable antenna for the 2.4-GHz WBAN application," *IEEE Trans. Antennas Propag.*, vol. 71, no. 2, pp. 1901–1906, Feb. 2023, doi: 10.1109/TAP.2022.3225529.

[39] S. Mudda, G. Km, and M. Mallikarjun, "Wide-band frequency tunable antenna for 4g, 5g/sub 6 GHz portable devices and MIMO applications," *Prog. Electromagn. Res. C*, vol. 118, pp. 25–41, 2022, doi: 10.2528/PIERC21112902.

[40] R. Hou, J. Ren, M. Zuo, X. Du, and Y. Z. Yin, "Magnetoelectric dipole filtering antenna based on CSRR with third harmonic suppression," *IEEE Antennas Wireless Propag. Lett.*, vol. 20, no. 7, pp. 1337–1341, Jul. 2021, doi: 10.1109/LAWP.2021.3080037.

[41] W.-A. Li, Z.-H. Tu, Q.-X. Chu, and X.-H. Wu, "Differential stepped-slot UWB antenna with common-mode suppression and dual sharp-selectivity notched bands," *IEEE Antennas Wireless Propag. Lett.*, vol. 15, pp. 1120–1123, 2016, doi: 10.1109/LAWP.2015.2496159.

[42] G. S. Reddy, A. Kamma, Sanjeev. K. Mishra, and J. Mukherjee, "Compact Bluetooth/UWB dual-band planar antenna with quadruple band-notch characteristics," *IEEE Antennas Wireless Propag. Lett.*, vol. 13, pp. 872–875, 2014, doi: 10.1109/LAWP.2014.2320892.

[43] K. Kota and L. Shafai, "Gain and radiation pattern enhancement of balanced antipodal Vivaldi antenna," *Electron. Lett.*, vol. 47, no. 5, p. 303, 2011, doi: 10.1049/el.2010.7579.

[44] S. Chamaani, M. S. Abrishamian, and S. A. Mirtaheri, "Time-domain design of UWB Vivaldi antenna array using multiobjective particle swarm optimization," *IEEE Antennas Wireless Propag. Lett.*, vol. 9, pp. 666–669, 2010.

[45] M. A. Pumallica-Paro, J. L. Arizaca-Cusicuna, and M. Clemente-Arenas, "A multiobjective genetic algorithm for analysis, design and optimization of antipodal Vivaldi antennas," in *Proc. IEEE-APS Topical Conf. Antennas Propag. Wireless Commun. (APWC)*, Sep. 2019, pp. 316–321, doi: 10.1109/APWC.2019.8870420.

[46] S. Lee, J. Hur, M.-B. Heo, S. Kim, H. Choo, and G. Byun, "A suboptimal approach to antenna design problems with kernel regression," *IEEE Access*, vol. 7, pp. 17461–17468, 2019, doi: 10.1109/ACCESS.2019.2896658.

[47] M.-A. Boujemaa, R. Herzi, F. Choubani, and A. Gharsallah, "UWB antipodal Vivaldi antenna with higher radiation performances using metamaterials," *Appl. Phys. A, Solids Surf.*, vol. 124, no. 10, pp. 1–7, Oct. 2018, doi: 10.1007/s00339-018-2132-1.

[48] V. K. Rai, M. Kumar, and S. P. Chakraborty, "A novel antipodal Vivaldi antenna with quad band notch characteristics for UWB applications," *Prog. Electromagn. Res. C*, vol. 120, pp. 119–133, 2022, doi: 10.2528/PIERC22022402.

[49] K. A. Alshamaileh, M. J. Almalkawi, and V. K. Devabhaktuni, "Dual band-notched microstrip-fed Vivaldi antenna utilizing compact EBG structures," *Int. J. Antennas Propag.*, vol. 2015, pp. 1–7, 2015, doi: 10.1155/2015/439832.

[50] Y. Xu, J. Wang, L. Ge, X. Wang, and W. Wu, "Design of a notched-band Vivaldi antenna with high selectivity," *IEEE Antennas Wireless Propag. Lett.*, vol. 17, no. 1, pp. 62–65, Jan. 2018, doi: 10.1109/LAWP.2017.2773707.

[51] W. Wang and Y. Zheng, "Improved design of the Vivaldi dielectric notch radiator with etched slots and a parasitic patch," *IEEE Antennas Wireless Propag. Lett.*, vol. 17, no. 6, pp. 1064–1068, Jun. 2018, doi: 10.1109/LAWP.2018.2832098.

[52] Z. Li, C. Yin, and X. Zhu, "Compact UWB MIMO Vivaldi antenna with dual band-notched characteristics," *IEEE Access*, vol. 7, pp. 38696–38701, 2019, doi: 10.1109/ACCESS.2019.2906338.

[53] D. M. Elsheakh and E. A. Abdallah, "Ultrawideband Vivaldi antenna for DVB-T, WLAN, and Wimax applications," *Int. J. Antennas Propag.*, vol. 2014, pp. 1–7, Jan. 2014, doi: 10.1155/2014/761634.

[54] R. Azim, M. T. Islam, H. Arshad, Md. M. Alam, N. Sobahi, and A. I. Khan, "CPW-fed super-wideband antenna with modified vertical bow-tie-shaped patch for wireless sensor networks," *IEEE Access*, vol. 9, pp. 5343–5353, 2021, doi: 10.1109/ACCESS.2020.3048052.

[55] H. H. Tran and H. C. Park, "Ultrawideband circularly polarized antenna with dual band-notched characteristics," *Int. J. RF Microwave Comput.-Aided Eng.*, vol. 29, no. 11, Nov. 2019, Art. no. e21911, doi: 10.1002/mmce.21911.

[56] A. Azari, A. Skrivervik, H. Aliakbarian, and R. A. Sadeghzadeh, "A super wideband dual-polarized Vivaldi antenna for 5G mmWave applications," *IEEE Access*, vol. 11, pp. 80761–80768, 2023, doi: 10.1109/ACCESS.2023.3300040.

NURHAYATI NURHAYATI (Member, IEEE) received the B.E., M.E., and D.E. degrees from Institut Teknologi Sepuluh Nopember (ITS), Surabaya, Indonesia, and the master's and Ph.D. degrees in telecommunication multimedia from the Department of Electrical Engineering, Faculty of Electrical Technology, ITS. She is currently a Lecturer with the Department of Electrical Engineering, Faculty of Engineering, Universitas Negeri Surabaya. She is also a Secretary with the Research Center, Institute for Research and Community Service, Universitas Negeri Surabaya. Her research interests include planar antenna, Vivaldi antenna, monopole antenna, wideband antenna, array antenna, radar antenna, and MIMO antenna. She has been a member of the Antennas and Propagation Society, since 2015, and the IEEE Young Professional Member, since 2018. In 2017, she received a scholarship from the International Publication Quality Improvement (PKPI), Kumamoto University, Kumamoto, Japan.

FITRI YULI ZULKIFLI (Senior Member, IEEE) received the bachelor's degree in electrical engineering from Universitas Indonesia (UI), in 1997, the M.Sc. degree from the Karlsruhe Institute of Technology, in 2002, and the Ph.D. degree in electrical engineering from UI, in 2009. Since 1998, she has been a Lecturer with the Department of Electrical Engineering, UI. Since 2017, she has also been a Professor in antenna and microwave engineering. She is currently a Researcher with the Antenna Propagation and Microwave Research Group (AMRG), UI, and the Director of the "Laboratory Prof. Fitri Yuli Zulkifli" and the UI Professional Engineering Study Program. She has won more than 40 research grants and has published more than 200 papers in journals/conference proceedings. Her research interests include antennas, propagation, microwaves, and communication.

EKO SETIJADI (Member, IEEE) was born in Indonesia, in 1972. He received the B.Eng. and M.Eng. degrees in electrical engineering from Institut Teknologi Sepuluh Nopember (ITS), Surabaya, Indonesia, and the Ph.D. degree in electrical engineering from Kumamoto University, Japan. He is currently an Associate Professor with the Department of Electrical Engineering, ITS. His current research interests include antenna design, microwave circuits, and metamaterials, particularly metasurface for communication and radar applications, electromagnetic compatibility, communication network design, and optimization,

BAGUS EDY SUKOCO was born in Solo, Indonesia, in 1971. He received the B.S. degree from the Department of Electrical Engineering, Universitas Jenderal Achmad Yani (UNJANI), Indonesia. He is currently with the Indonesian Institute of Sciences/Lembaga Ilmu Pengetahuan Indonesia (LIPI), now known as the National Research and Innovation Agency in the Telecommunication and Electronics Research Center (PPET), Bandung, Indonesia. His research interests include radar antenna and antenna measurement.

MOHD NAJIB MOHD YASIN (Senior Member, IEEE) received the M.Eng. and Ph.D. degrees from The University of Sheffield, U.K., in 2007 and 2013, respectively, he has established a reputation for excellence in his field, with an academic foundation rooted. He is a distinguished Associate Professor at Universiti Malaysia Perlis, has carved a niche for himself in the electronic engineering discipline. His expertise spans across vital areas such as computational electromagnetics, conformal antennas, and the intricacies of mutual coupling in antenna arrays, with a special focus on dielectric resonator antennas, showcasing his commitment to advancing wireless communication technologies. He foray into the cutting-edge domain of reconfigurable intelligent surfaces (RIS) underscores his role as a trailblazer in electronic engineering. This innovative research avenue, which seeks to revolutionize wireless communications by dynamically manipulating electromagnetic waves, highlights his dedication to pioneering advancements that could redefine the industry's future. In addition to his technical prowess, and affiliation with the IEEE as a Senior Member further accentuates his esteemed standing within the engineering community, reflecting his significant contributions and professional maturity in the field. His contributions extend beyond mere academic achievements, as they embody a profound impact on the technological landscape of wireless communications, making him a pivotal figure in the academic and professional realms of electronic engineering.

ALEXANDRE MANICOBA DE OLIVEIRA (Member, IEEE) received the bachelor's degree in electrical engineering modality computing from the Catholic University of Santos, and the master's and Ph.D. degrees in electrical engineering sciences from the Polytechnic School, University of São Paulo, Brazil. He is currently a Professor with the Maxwell Laboratory of Microwave and Applied Electromagnetism, Federal Institute of São Paulo, Brazil. His research interests include antipodal Vivaldi antenna, microwave imaging, near-field antenna imaging, radar, electronics, and ultra-wideband antenna. He is a member of the Brazilian Society of Electromagnetism (SBMag) and SBMO.